J. Radiat. Res., 52, 766–774 (2011)

Persistence and Dynamics of DNA Damage Signal Amplification Determined by Microcolony Formation and Live-cell Imaging

Yasuyoshi OKA, Motohiro YAMAUCHI, Masatoshi SUZUKI, Shunichi YAMASHITA and Keiji SUZUKI*

DNA damage response/DNA damage foci/Live-cell imaging.

Cell cycle checkpoints are essential cellular process protecting the integrity of the genome from DNA damaging agents. In the present study, we developed a microcolony assay, in which normal human diploid fibroblast-like cells exposed to ionizing radiation, were plated onto coverslips at very low density (3 cells/cm^2). Cells were grown for up to 3 days, and phosphorylated ATM at Ser1981 and 53BP1 foci were analyzed as the markers for an amplified DNA damage signal. We observed a dose-dependent increase in the fraction of non-dividing cells, whose increase was compromised by knocking down p53 expression. While large persistent foci were predominantly formed in non-dividing cells, we observed some growing colonies that contained cells with large foci. As each microcolony was derived from a single cell, it appeared that some cells could proliferate with large foci. A live-imaging analysis using hTERT-immortalized normal human diploid cells transfected with the EGFP-tagged *53BP1* gene revealed that the formation of persistent large foci was highly dynamic. Delayed appearance and disappearance of large foci were frequently observed in exposed cells visualized 12–72 hours after X-irradiation. Thus, our results indicate that amplified DNA damage signal could be ignored, which may be explained in part by the dynamic nature of the amplification process.

INTRODUCTION

Exposure of mammalian cells to ionizing radiation (IR) gives rise to a range of DNA lesions including DNA double-strand breaks (DSBs). Production of DSBs results in activation of G_1/S, intra-S and G_2/M checkpoints,[1–5] by which the genome integrity is secured. A central player in cell cycle checkpoints is the ataxia-telangiectasia mutated (ATM) protein. In fact, cells derived from AT patients show multiple cell cycle checkpoint defects, which lead to chromosomal instability, hypersensitization to IR and predisposition to cancer.[6–9] It is demonstrated that ATM exists as a dimer or a higher-order multimer in unstressed human cells, and it dissociates into monomers in response to alterations in chromatin conformation caused by DSBs.[10] The dissociated ATM is autophosphorylated at Ser1981, and thus, activated ATM phosphorylates many proteins, such as histone H2AX, NBS1, 53BP1, MDC1, SMC1 and p53, which are the mediators and effectors of cell cycle checkpoints.[8,9,11] Several previous studies reported that DNA damage checkpoint factors were locally phosphorylated or accumulated at the chromatin regions flanking DSB sites, and they formed discrete foci, which were detectable microscopically.[12–15] Thus, activation of a DNA damage checkpoint is now visualized by DNA damage checkpoint foci.

Previously, it was demonstrated that the number of the initial foci decreased concurrently with DSB repair, while some fraction of the initial foci remained for a long time after the initial insult.[12,15] We and others have found that such persistent foci became large in size, and that the large foci were essential for DNA damage signal amplification.[13,15] In fact, the foci size was positively correlated with the phosphorylation level of p53, and cells from genetic disorders with a defect in creating large foci showed improper cell cycle arrest. We also found that large foci were rarely detected in cells progressed to S-phase after X-irradiation. Therefore, we concluded that large foci, which represent amplified DNA damage checkpoint signal, should be sufficient for executing proper cell cycle arrest.

While these results were in agreement with the general idea that a DNA damage checkpoint is essential for the maintenance of genome integrity, it should be pointed out that a certain fraction of cells progressed to S-phase even with large

*Corresponding author: Phone: +81-95-819-7116,
Fax: +81-95-819-7116,
E-mail: kzsuzuki@nagasaki-u.ac.jp
Atomic Bomb Disease Institute, Graduate School of Biochemical Sciences, Nagasaki University, 1-12-4 Sakamoto, Nagasaki 852-8523, Japan.
doi:10.1269/jrr.10164

foci,[15] indicating that there are circumstances, in which DNA damage signal is ignored. Similar observations were reported in a recent study, which indicated a limitation of the G1 checkpoint.[16] In that study, cells could be released from G1 arrest with γ-H2AX foci and chromosome aberrations present. These results encouraged us to design experiments, in which propagation of a single cell with large foci could be pursued. In the present study, we have developed a single-cell based microcolony assay using normal human diploid cells, which allows us to detect large foci in the progeny of a single cell. In addition, live-cell imaging of EGFP-tagged 53BP1 foci enables us to reveal appearance and disappearance of large foci, which associate with the dynamics of DNA damage signal amplification.

We observed a dose-dependent increase in the fraction of non-dividing cells, whose increase was compromised by knocking down p53 expression by shRNA. While large persistent foci were predominantly formed in non-dividing cells, we observed large foci in some cells within slowly- and rapidly-growing microcolonies. Thus, it appeared that some cells could proliferate even with large foci. A live-imaging analysis using normal human diploid cells transfected with the EGFP-tagged *53BP1* gene revealed that foci disappearance and delayed foci appearance were more frequent in X-irradiated cells than the control cells. Our results indicate that an amplified DNA damage signal can be ignored, which may be explained in part by the temporal dynamics of the process of DNA damage signal amplification.

MATERIALS AND MEHODS

Cell culture and X-irradiation

Normal human diploid fibroblast-like (HE49) cells[17] and hTERT-immortalized normal human BJ1 fibroblasts (BJ1-hTERT) cells were cultured in minimal essential Eagle's media (MEM) containing 10% fatal bovine serum (ThermoTrace Ltd., Australia) as described previously.[17] Cells (4×10^5) were subcultured in T25 flasks (25 cm^2) to maintain exponential growth. Cells were irradiated with X-rays from an X-ray generator at 150 kVp and 5 mA with a 0.1 mm copper filter at a dose rate of 0.492 Gy/min. Immediately after X-irradiation, cells were collected by trypsinization, and the number of cells were counted. For standard survival assays, cells were plated onto 100 mm dishes in order to make 100 surviving colonies, and grown for 10 days in a CO_2 incubator. For microcolony assays, cells were plated onto coverslips at low density (3 cells/cm^2). Then, they were allowed to form microcolonies in a CO_2 incubator. For BrdU-staining, microcolonies formed by 3 days after X-irradiation were further grown in a medium containing 10 μM BrdU and 1 μM FldU for 3 days.

Immunofluorescence staining

For immunofluorescence staining, cells were washed with phosphate-buffered saline (PBS), fixed with 4% formaldehyde in PBS for 10 min, and permeabilized with 0.5% Triton X-100 in PBS for 5 min on ice. Then, the cells were incubated with mouse monoclonal anti-phosphorylated ATM at Ser1981 antibody (Clone 10H11.E12, Rockland, PA) and anti-53BP1 antibody (Bethyl, TX) diluted in TBS-DT (20 mM Tris-HCl, 137 mM NaCl, pH 7.6, containing 5% skim milk and 0.1% Tween20) for 2 hours at 37°C. The primary antibodies were detected by incubating cells with the secondary antibody conjugated with Alexa488 or Alexa594 (Molecular Probes) for 1 hour at 37°C. After incubation, cells were washed with PBS and counterstained with 0.1 mg/ml of DAPI. For the detection of BrdU, microcolonies were washed with PBS, fixed with 100% methanol for 5 min, and treated with 1N HCl for 30 min. Then, the microcolonies were incubated with mouse monoclonal anti-BrdU antibody (clone BMC-9318, Roche Applied Science) diluted in TBS-DT for 2 hours at 37°C. The primary antibodies were detected by incubating cells with the secondary antibody conjugated with Alexa488 (Molecular Probes) for 1 hour at 37°C. After incubation, cells were washed with PBS and counterstained with 0.1 mg/ml of DAPI.

The digital images were captured by the fluorescence microscopy DM6000B (Leica, Tokyo), and they were analyzed by the image-processing software FW4000 (Leica, Tokyo). The diameters of phosphorylated ATM at Ser1981 and 53BP1 foci were calculated using Adobe Photoshop 7.0. First, the size of the focus was acquired as the total number of pixels by marking each focus. Next, the gross area of the focus was estimated by combining the total number of pixels and the unit area of a pixel (0.026 μm^2). Finally, the focus diameter was calculated based on the gross area by considering that the focus was circular.

Knockdown of p53 by shRNA

Two synthetic oligonucleotides were obtained from Sigma-Aldrich Japan. The sequences of the sense and anti-sense strands were as follows: 5'-caccgactccagtggtaatctacttcaagagagtagattaccactggagtc-3' and 5'-aaaagactccagtggtaatctactctcttgaagtagattaccactggagtc-3'. They were annealed and ligated into pENTR/H1/TO vector (Invitrogen) to construct pENTR/H1/TO/sh-p53. BJ1-hTERT cells were transfected with pENTR/H1/TO/sh-p53 using electroporation and stable clones were selected by culturing cells in a medium containing 50 μg/ml of Zeocine (Invitrogen).

Western blot analysis

Western blotting was performed as previously described.[15] Briefly, exponentially growing cells were lysed in lysis buffer (50 mM Tris-HCl (pH 7.2), 150 mM NaCl, 1% NP-40, 1% sodium deoxycholate, and 0.1% SDS) containing 1 mM 4-(2-aminoethyl)-benzensulfonyl fluoride hydrochloride. The cell lysate was sheared through 28 G needle 5 times and cleared by centrifugation at 15,000 rpm for 10 min at 4°C. Then, the supernatant was collected and used as total

cellular protein. Total protein concentration was determined by the BCA protein assay (Pierce, Rockford, IL). Proteins (16 μg) were electrophoresed through an SDS-polyacrylamide gel and were electrophoretically transferred to a polyvinyl difluoride membrane in transfer buffer (100 mM Tris, 192 mM glycine). After overnight incubation with blocking solution (10% skim milk), the membrane was incubated with anti-p53 monoclonal antibody (clone Bp53-12, NeoMarkers), a biotinylated anti-mouse IgG antibody, and streptavidine-alkaline phosphatase. The bands were visualized after addition of nitroblue tetrazolium/5-bromo-4-chloro-3-indolyl phosphate as a substrate.

Live-cell imaging

HE49 cells were transiently transfected with the plasmid containing the EGFP-tagged mouse *53BP1* gene using electroporation (The EGFP-53BP1 plasmid was kindly provided by Dr. Yasuhisa Adachi).[18] Cells were grown for 48 hours, collected by trypsinization, and replated onto glass-bottom 35-mm dish. Then, they were grown for further 24 hours before X-irradiation. Immediately after X-irradiation, the 35-mm dishes were placed in an incubation chamber equipped with a time-lapse imaging system (BioStation-ID, GE Healthcare Japan). Both phase contrast and fluorescence images were acquired simultaneously every 3 minutes. For EGFP fluorescence, a B-2A filter block (GE Healthcare Japan) was used. To avoid the possibility of illumination-induced toxicity, light output was reduced by neutral density gray filters and exposure time was set to 1/20 second. This imaging condition did not cause any artificial foci when the samples that were exposed for live-cell imaging were compared with those without exposure to any excitation light.

Data analysis

A two-tailed *Mann-Whitney* test was used to evaluate differences between the control and irradiated cells. A *P* value of less than 0.05 was considered significant difference.

RESULTS

Normal human diploid cells, HE49 cells, were derived from mesenchymal tissue with fibroblast-like morphology. These cells are highly proliferative in culture as described

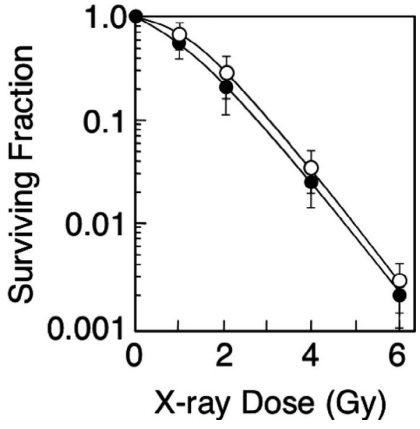

Fig. 1. Survival curves for HE49 and BJ1-hTERT cells. Exponentially growing cells were exposed to various doses of X-rays. Immediately following irradiation, cells were counted and seeded at limiting dilution onto 100-mm dishes, and grown for 10 days. Colonies with more than 50 cells were counted. The results were obtained from three independent experiments. Closed circle; HE49, open circle; BJ1-hTERT. Data indicate the mean ± SEM.

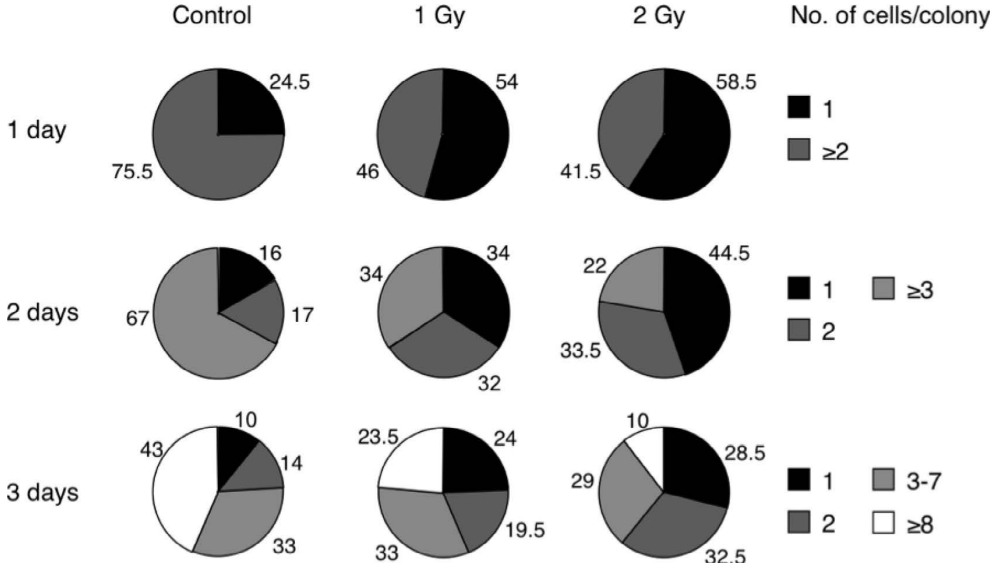

Fig. 2. Formation of microcolonies by the control and X-irradiated cells. Exponentially growing HE49 cells were exposed to 1 Gy or 2 Gy of X-rays, replated at a low density, and grown for up to 3 days. Two hundred initial cells were examined. Numbers indicate the percentage of colonies in each category.

previously.[17] The survival curve for HE49 cells is shown in Fig. 1. In the present study, we used 1 Gy and 2 Gy of X-rays, which gave 0.6 and 0.2 surviving fractions, respectively, in standard colony forming assays. In addition, cells were plated onto coverslips at very low density (3 cells/cm^2) shortly after exposure, and grown for up to 3 days. Since synchronization by itself increases spontaneous foci, we decided to use asynchronous cells. The effect of radiation dose and time post-exposure on the number of cells within individual microcolonies is shown in Fig. 2. Approximately half of the control cells formed microcolonies with 8 cells or more at day 3, and these colonies were classified as rapidly-growing microcolonies. One-forth of the control cells made microcolonies consisting of 3–7 cells, which were designated as slowly-growing microcolonies. The remaining one-forth of the initially-seeded cells remained as single cell or as two celled colonies even after 3-days of incubation, and they were classified as non-dividing cells. Considering that the cloning efficiency of HE49 cells is approximately 30%, it is most likely that the rapidly-growing microcolonies are the source of colonies with 50 cells or more in a standard colony-forming assay.

A dose-dependent increase of non-dividing cells was observed in X-ray-irradiated cells (Fig. 2). While the fraction of non-dividing cells in the control population was 24% at day 3, it was approximately 44% and 60% in 1 Gy- and 2 Gy-exposed populations, respectively. Conversely, the percentage of rapidly-growing microcolonies showed a dose-dependent decrease. As ionizing radiation is well known to induced temporal cell cycle arrest or cell cycle delay, the proliferative capacity of cells within microcolonies was determined by growing them in a medium containing BrdU from 3 days after X-irradiation. As shown in Table 1, rapidly-growing microcolonies are all BrdU-positive, while the fraction of BrdU-positive slowly-growing microcolonies is half or less, depending on the radiation dose. In general, we observed that BrdU-positive slow-growing microcolonies consisted of more cells than BrdU-negative microcolonies. We also confirmed that all non-dividing cells were BrdU-negative. These results indicate that cells forming slow-growing microcolonies could continue cell proliferation for

Table 1. Percentage of BrdU-positive microcolonies

Cells	No. colonies analyzed	No. of BrdU-positive colonies		
		Non-dividing	Slowly-growing	Rapidly-growing
Control	50	0/12	8/16	22/22
1 Gy	50	0/22	3/16	12/12
2 Gy	5	0/31	2/15	4/4

Microcolonies formed after 3-days incubation were stained with BrdU for further 3 days. Colonies, in which at least half of the cells showed BrdU incorporation, were counted as BrdU-positive colonies.

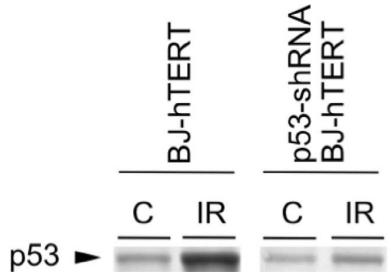

Fig. 3. Suppression of p53 by shRNA-expressing vector. Wild-type BJ1-hTERT cells and BJ1-hTERT cells that were stably transfected with the vector containing shRNA for the human p53 gene were exposed to 6 Gy of X-irradiation (IR). The level of expression of p53 was determined 2 hours post-irradiation by Western blotting, as described in Materials and Methods. C; control cells, IR; 6 Gy of X-rays.

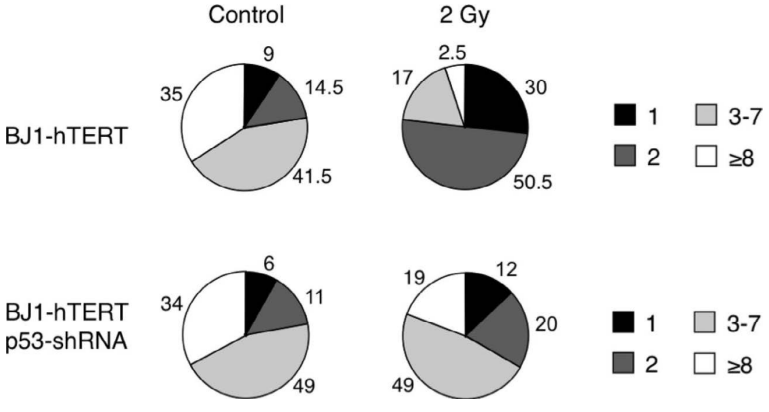

Fig. 4. Formation of microcolonies by the control and X-irradiated cells. Exponentially growing BJ1-hTERT cells were exposed to 2 Gy of X-rays, replated at a low density, and grown for 3 days. Two hundred initial cells were examined. Numbers indicate the percentage of colonies in each category.

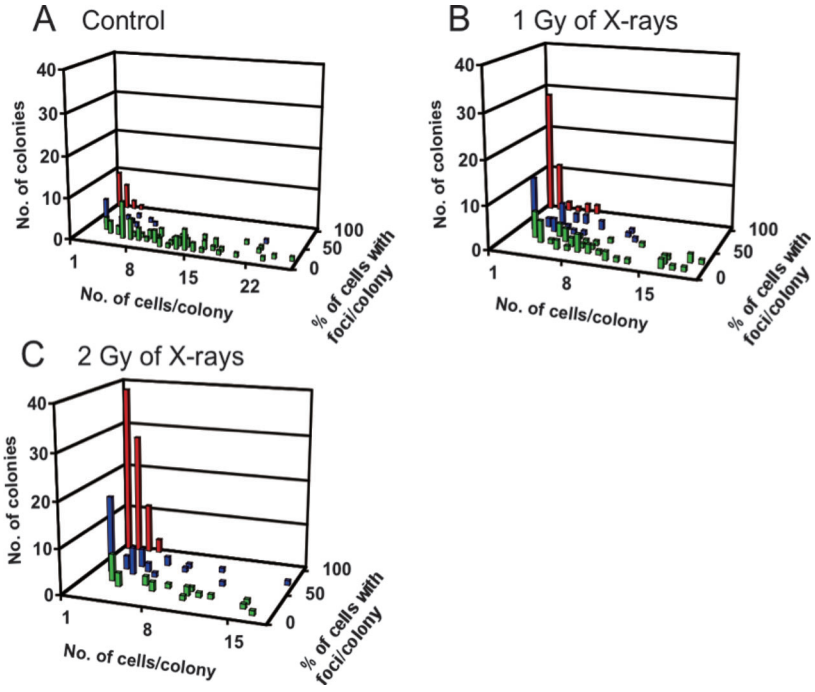

Fig. 5. Relationship between foci formation and microcolony formation. Exponentially growing HE49 cells were irradiated with 1 or 2 Gy of X-rays, replated at a low density, and grown for 3 days before fixation. Immunofluorescence staining for phosphorylated ATM at Ser1981 and 53BP1 foci was performed as described in Materials and Methods. Cells with foci, whose diameter was 1.2 μm or more, were counted as foci-positive cells. Two hundred initial cells were counted in each dose. Panels A, B and C represent the control cells, cells exposed to 1 Gy or 2 Gy of X-rays, respectively. Green bars indicate microcolonies in which less than 50% of cells were foci-positive. Blue bars indicate microcolonies, in which the fraction of foci-positive cells was 50% or more. Red bars indicate foci-positive non-dividing cells or microcolonies consist of foci-poisitive cells.

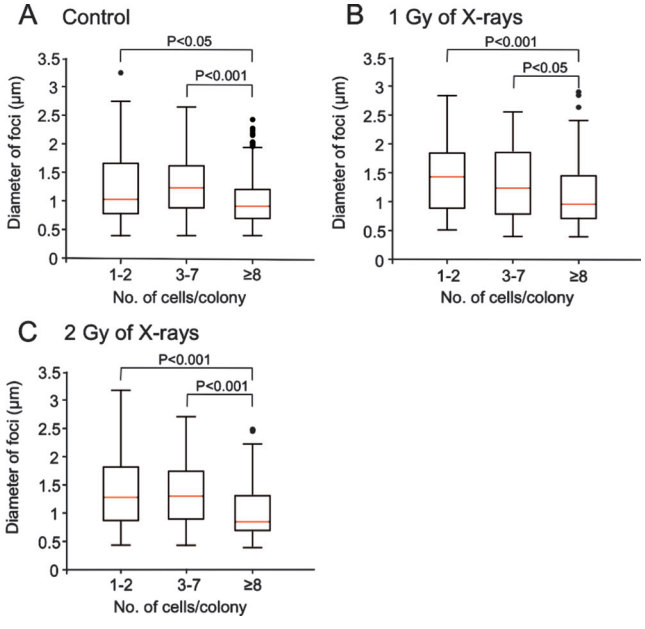

a few days after X-irradiation, but they gradually terminate their growth thereafter. According to the results shown in Fig. 1, surviving fractions of HE49 cells with 1 Gy and 2 Gy of X-rays were 0.6 and 0.2, respectively. Therefore, it seems likely that rapidly-growing microcolonies give rise to those judged as colonies by clonogenic assay.

The involvement of a p53-dependent DNA damage signal in growth arrest was examined by knocking-down p53 expresion. For this purpose, we have established BJ1-

Fig. 6. Distribution of the size of colocalized foci. Exponentially growing HE49 cells were irradiated with 1 or 2 Gy of X-rays, replated at a low density, and grown for 3 days before fixation. Diameter of the foci of phosphorylated ATM/53BP1 was calculated as described in Materials and Methods. Two hundred initial cells were counted in each dose. Panels A, B and C represent the control cells, cells exposed to 1 Gy or 2 Gy of X-rays, respectively. Boxes indicate boundaries of the 25th percentile to the 75th percentile. The red line indicates the median of the data and error bars indicate the spread of the data. *P* values were obtained by two-tailed *Mann-Whitney* test.

hTERT cells transfected with the vector expressing shRNA for p53. As shown in Fig. 3, we have confirmed that p53 accumulation in response to 6 Gy of X-rays was significantly compromised in p53 knock-down cells compared with the parental BJ1-hTERT cells. The cells were exposed to 2 Gy of X-rays, which gave approximately 0.3 surviving fraction (Fig. 1). For unirradiated cells, the percentages of growing microcolonies were almost the same for p53 knock-down cells and for the parental BJ1-hTERT cells (Fig. 4). After X-irradiation, microcolony formation was severely inhibited in the parental BJ1-hTERT cells, and more than 80% of them were non-dividing cells. In contrast, p53 knock-down cells showed only a slight increase in the fraction of non-dividing cells, indicating that a p53-dependent pathway was involved in the increase of non-dividing cells in response to X-irradiation.

The amplification of a DNA damage signal in cells within microcolonies was visualized by large foci of phosphorylated ATM at Ser1981 and 53BP1. Since we found that some phosphorylated ATM and 53BP1 foci were not co-localied, we only counted those phosphorylated ATM foci that were co-localized with 53BP1 foci. As the median of the focus diameter was 1.2 μm 3 days after irradiation, we categorized those foci, whose diameter was 1.2 μm or more, were large foci. As shown in Table 2, approximately 40% of microcolonies formed by the control cells were foci-negative, whereas the number of foci-negative microcolonies decreased upon X-irradiation. In order to determine whether growing microcolonies persist amplified DNA damage signal or not, foci-positive microcolonies were analyzed 3 days after X-irradiation (Fig. 5). We counted the number of cells consisting within each microcolony as well as the percentage of cells with large foci. In the control cells, approximately half of non-dividing cells were foci-positive, and the fraction of foci-positive non-dividing cells was dramatically increased by X-irradiation. Foci-positive cells were also observed in both slow-growing and rapidly-growing microcolonies formed by the control cells, and X-irradiation increased the percentage of foci-positive cells in both types of microcolonies. Although we never observed rapidly-growing microlonies, in which all cells were foci-positive, some rapidly frowing microcolonies had foci-positive cells within them. The distribution of foci sizes for non-dividing cells, slowly-growing colonies, and rapidly growing cells is compared in Fig. 6. The median foci diameter in rapidly-growing colonies was smaller than those observed in non-dividing cells and slowly-growing colonies, however, some large foci were detectable even in the rapidly-growing cells. These

Table 2. Percentage of foci-negative microcolonies

Cells	No. colonies analyzed	No. of foci-negative colonies (%)	
		Slowly-growing	Rapidly-growing
Control	173	33 (19.1)	33 (19.1)
1 Gy	164	18 (11.0)	15 (9.1)
2 Gy	160	13 (8.1)	5 (3.1)

Microcolonies formed after 3-days incubation were analyzed. Colonies, in which at least one cell showed foci, were counted as foci-positive colonies.

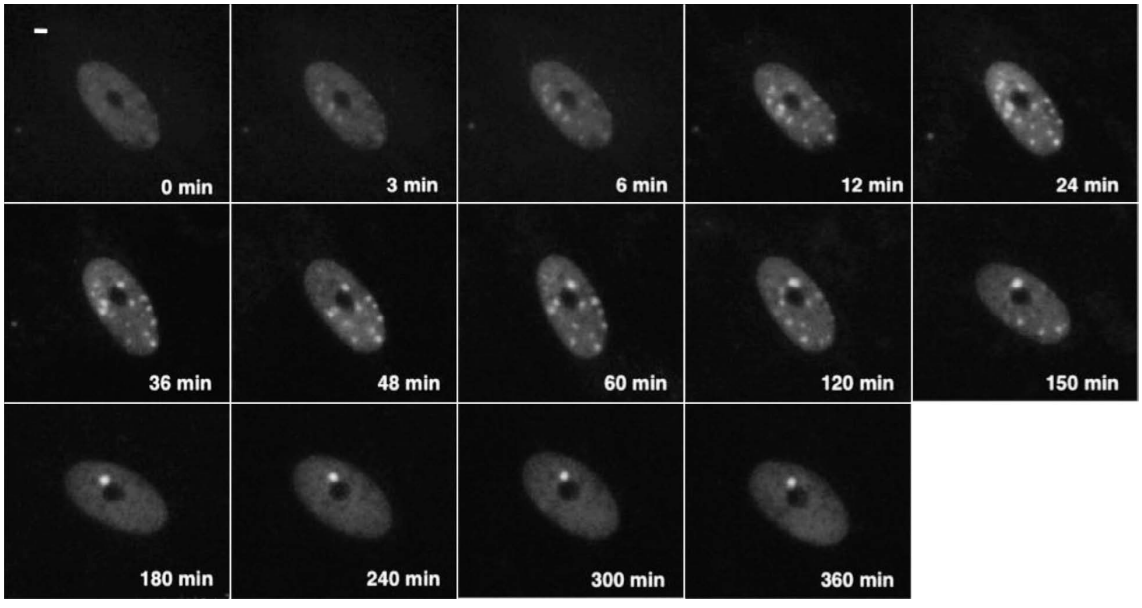

Fig. 7. Live-cell imaging analysis of the initial foci. HE49 cells were transfected with the EGFP-tagged mouse *53BP1* gene as described in Materials and Methods. The control cells and cells irradiated with 0.5 Gy of X-rays were grown for 6 hours, and digital images were acquired every 3 minutes. As it took 5 minutes after X-irradiation before the imaging was started, time 0 min indicated 5 minutes after X-irradiation. Bar indicates 5 μm.

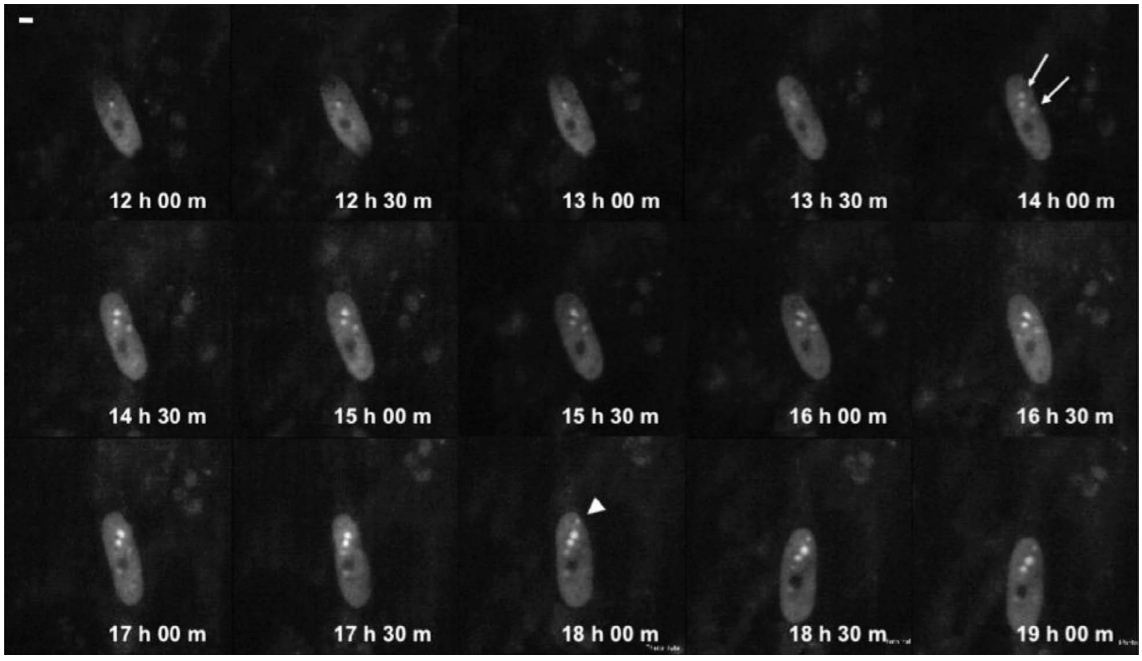

Fig. 8. Live-cell imaging analysis of large persistent foci. HE49 cells were transfected with the EGFP-tagged mouse *53BP1* gene as described in Materials and Methods. The control cells and cells irradiated with 2 Gy of X-rays were grown for 72 hours after X-irradiation, and digital images were acquired every 3 minutes. Two white arrows and an arrow head indicate the foci showing dynamics. Bar indicates 5 μm.

results indicate that cells harboring large foci still have a chance to proliferate, suggesting that an amplified DNA damage signal could be ignored or overridden.

Since the size of residual foci in microcolonies varied, we examined the dynamics of foci size using live-cell imaging. For this purpose, we used HE49 cells expressing EGFP-tagged 53BP1 protein. As shown in Fig. 7, 53BP1 foci were detectable as bright dots in the nucleus. Since 5 minutes were required before starting the imaging, the "0 minute" time-point in Fig. 7 is actually 5 minutes after X-irradiation. The initial foci became detectable within 3 minutes after X-irradiation, and the maximum foci number was observed 30 minutes ~ to one hour after irradiation. At later time-points, the number of foci gradually decreased, and a few foci persisted as residual foci. These residual foci were large in size. The dynamics of residual foci formation was examined from 12 and 72 hours after X-irradiation. We found that the formation of residual foci was highly dynamic. For example, during the 7 hours between 12 and 19 hours after 2 Gy of X-rays, we observed the delayed appearance of three foci, although one focus that appeared at 18 hours was not a large focus (Fig. 8). As summarized in Table 3, out of 50 cells examined, the disappearance of large foci was detected in 7 cells, while 11 cells showed a delayed appearance of large foci between 12 and 72 hours after 2 Gy of X-rays. During the post-irradiation imaging period, we did not observe cell division in any cells with large foci.

Table 3. Dynamics of persistent activation of cell cycle checkpoint

Cell	No. cells analyzed	No. fo foci		
		Persisted	Disappeared	Appeared
Control	100	8	0	1
2 Gy	100	43	7	11

Foci of EGFP-53BP1 was examined by the live-cell imaging system, and they were subjected to time-lapse analysis. The analysis was performed between 12 and 72 hours after irradiation. Foci, whose diameter was more than 1.2 mm, were analyzed.

DISCUSSION

DNA damage checkpoints have been generally believed to be a crucial mechanisms to guard the integrity of the genome.[1–5] In particular, the G1 checkpoint is indispensable for securing continuous growth arrest of cells with unrepaired DNA damage. Accordingly, our results also confirmed that p53 is involved in the increase of non-dividing cells in response to X-irradiation (Fig. 4). Apparently, X-irradiation increased the fraction of non-dividing cells with large foci. We found that these non-dividing cells became positive for senescence-associated β-galactosidase staining 6 days after X-irradiation (data not shown), indicating that

they demonstrated an induced senescence-like growth arrest as described previously.[19,20)]

While activation of a DNA damage checkpoint plays a pivotal role in executing cell cycle arrest, a recent report demonstrated that some DNA damage checkpoints were imperfect.[16)] In the present study, we developed a single-cell base microcolony assay, which enabled us to examine whether cells with large foci could proliferate. As shown in Fig. 5, we observed large foci in cells within microcolonies. Although we never found rapidly-growing microcolonies, in which 100% of cells contained large foci-positive, foci-positive cells were detectable not only in the cells within slowly-growing microcolonies but also in rapidly-growing microcolonies. However, the percentage of foci-positive cells was higher in slowly-growing microcolonies, and it was over 50% in some slowly-growing microcolonies. These results suggest that some cells were able to proliferate with large foci.

Since the G1 checkpoint has been shown as a guardian of genome integrity, how can the imperfect nature of this checkpoint be explained? As the foci size showed variation in the cells within the microcolonies, it seemed possible that foci formation might be variable in nature. Cells with smaller foci may proliferate, suggesting that a "threshold" may exist for the DNA damage signal to activate the checkpoint. Such a threshold was reported for activation of the G2 checkpoint.[5,21,22)] Thus, it seemed possible that a similar threshold could exist for G1 checkpoint activation. If so, foci size might be an important determinant of checkpoint activation. In the present study, we have considered cells as foci-positive, if they contained a focus, whose diameter was 1.2 μm or greater. As the intensity of DNA damage signal was well correlated with the size of the foci,[15)] it is possible that DNA damage signal was not sufficient for cell cycle arrest, if the foci size was changeable. While the mean foci size was smaller in cells within rapidly-growing microcolonies than in non-dividing cells and those in slowly-growing microcolonies, the distribution of their size was highly variable (Fig. 6). Thus, one possibility is that persistent amplification of DNA damage signal is so dynamic that it sometimes fails to activate cell cycle arrest.

As we reported previously, the size of the initial foci was changeable.[15)] Within the first 30 minutes, the foci size were increased drastically, and then, residual foci continued to grow their size. Therefore, we applied the live-cell imaging analysis to visualize the dynamics of persistent large foci formation using EGFP-tagged 53BP1 protein. We could detect immediate formation of a localized EGFP signal, which was colocalized with the endogenous 53BP1 foci. Persistent foci became apparent several hours after X-irradiation (Figs. 7 and 8), and dynamic formation of residual foci was observed thereafter. We saw both delayed appearance and disappearance of foci predominantly in cells exposed to radiation, indicating that such foci dynamics could explain, in part, why an amplified DNA damage signal was ignored. Although we were unable to detect the division of cells with foci, the dynamics of foci formation and disappearance could be detected in a substantial number of cells after X-irradiation.

There are two remaining questions that should be addressed. One is the mechanism of foci dynamics. As the foci formation is dependent on phosphorylation of the foci factors,[12–15)] it is assumed that ATM activation by itself is dynamic. Since ATM is activated through alterations in higher-order chromatin structure,[10)] foci dynamics may reflect changes in chromatin organization.[23)] In fact, recent studies have indicated that foci formation is influenced by heterochromatin organization[24,25)] as well as histone modifications.[26–30)] Therefore, the dynamic change in chromatin structure in exposed cells should affect foci formation. The second possibility is that delayed foci induction was caused by radiation-induced genomic instability. It is well known that ionizing radiation induces non-targeted effects in the progeny of cells surviving ionizing radiation, which results in delayed formation of DNA double strand breaks in surviving cells.[31–34)] Thus, delayed DNA breaks could be one reason leading to the delayed appearance of foci. The other question is about the molecular nature of persistent large foci. Since chromosome breaks were detected in cells 24 hours after radiation exposure, persistent large foci could represent remaining DNA breaks. Unrepaired DNA breaks may not always be recognized as DNA damage, as it has been suggested that ATM and its downstream factors might hold two broken ends together.[35,36)] As ionizing radiation creates clustered complex damage,[37–40)] which is difficult to repair, a fraction of complex DNA damage could persist for a long time after radiation exposure. These possibilities should be examined in the future experiments.

In summary, our present study demonstrated that amplification of DNA damage signal can be ignored or bypassed, which may be explained in part by the kinetics of appearance and disappearance of the signal, as presented by the foci formation. Importantly, the number of large foci in cells might be very limited when cells are exposed to lower doses of radiation. Under such circumstances, the amplification of a DNA damage signal is critical for executing cell cycle arrest. Thus, the dynamics of DNA damage signaling should considered when assessing the likelihood of checkpoint activation.

ACKNOWLEDGEMENT

This work was supported by the Global Center Of Excellence (GCOE) program in Nagasaki University. We thank Dr. Yasuhisa Adachi for providing us the EGFP-53BP1 plasmid. YO greatly appreciates Dr. Masao Tomonaga for the continuous help and support.

REFERENCES

1. Hartwell LH and Kastan MB (1994) Cell cycle control and

cancer. Science **266**: 1821–1828.
2. Zhou BB and Elledge SJ (2000) The DNA damage response: putting checkpoints in perspective. Nature **408**: 433–439.
3. Kastan MB and Bartek J (2004) Cell-cycle checkpoints and cancer. Nature **432**: 316–323.
4. Jeggo PA and Lobrich M (2006) Contribution of DNA repair and cell cycle checkppoint arrest to the maintenance of genomic stability. DNA repair **5**: 1192–1198.
5. Lobrich M and Jeggo PA (2007) The impact of a negligent G2/M checkpoint on genomic instability and cancer induction. Nat Rev Cancer **7**: 861–869.
6. Jackson SP (1995) Ataxia-telangiectasia at the crossroads. Curr Biol **5**: 1210–1212.
7. Meyn MS (1995) Ataxia-telangiectasia and cellular responses to DNA damage. Cancer Res **55**: 5591–6001.
8. Shiloh Y (2003) ATM and related protein kinases: safeguarding genome integrity. Nat Rev Cancer **3**: 155–168.
9. Lavin MF (2008) Ataxia-telangiectasia: from a rare disorder to a paradigm for cell signalling and cancer. Nat Rev Mol Cell Biol **9**: 759–769.
10. Bakkenist CJ and Kastan MB (2003) DNA damage activates ATM through intermolecular autophosphorylation and dimer dissociation. Nature **421**: 499–506.
11. Matsuoka S, *et al* (2007) ATM and ATR substrate analysis reveals extensive protein networks responsive to DNA damage. Science **316**: 1160–1166.
12. Paull TT, *et al* (2000) A critical role for histone H2AX in recruitment of repair factors to uclear foci after DNA damage. Curr Biol **10**: 886–895.
13. Bekker-Jensen S, *et al* (2006) Spatial organization of the mammalian genome surveillance machinery in response to DNA strand breaks. J Cell Biol **173**: 195–206.
14. Stucki M and Jackson SP (2006) gamma H2AX and MDC1: anchoring the DNA-damage-response machinery to broken chromosomes. DNA repair **5**: 534–543.
15. Yamauchi M, *et al* (2008) Growth of persistent foci of DNA damage checkpoint factors is essential for amplification of G1 checkpoint signaling. DNA repair **7**: 405–417.
16. Deckbar D, *et al* (2010) The limitation of the G1-S checkpoint. Cancer Res **70**: 4412–4421.
17. Watanabe M, *et al* (1992) Effect of multiple irradiation with low doses of gamma-rays on morphological transformation and growth ability of human embryo cells in vitro. Int J Radiat Biol **62**: 711–718.
18. Jullien D, *et al* (2002) Kinetochore localisation of the DNA damage response component 53BP1 during mitosis. J Cell Sci **115**: 71–79.
19. Beausejour CM, *et al* (2003) Reversal of human cellular senescence: roles of the p53 and p16 pathways. EMBO J **22**: 4212–4222.
20. Suzuki K, *et al* (2001) Radiation-induced senescence-like growth arrest requires TP53 function but not telomere shortening. Radiat Res **155**: 248–253.
21. Deckbar D, *et al* (2007) Chromosome breakage after G2 checkpoint release. J Cell Biol **176**: 749–755.
22. Ishikawa A, *et al* (2010) Image-based quantitative determination of DNA damage signal reveals a threshold for G2 checkpoint activation in response to ionizing radiation. Genome Integr **1**: 10.
23. Misteli T and Soutoglou E (2009) The emerging role of nuclear architecture in DNA repair and genome maintenance. Nat Rev Mol Cell Biol **10**: 243–254.
24. Goodarzi AA, *et al* (2008) ATM signaling facilitates repair of DNA double-strand breaks associated with heterochromatin. Mol Cell **31**: 167–177.
25. Noon AT, *et al* (2010) 53BP1-dependent robust localized KAP-1 phophorylation is essential for heterochromatic DNA double-strand break repair. Nat Cell Biol **12**: 177–184.
26. Downs JA (2008) Histone H3 K56 acetylation, chromatin assembly, and the DNA damage checkpoint. DNA repair **7**: 2020–2024.
27. Galantly Y, *et al* (2009) Mammalian SUMO E3-ligase PIAS1 and PIAS4 promote responses to DNA double-strand breaks. Nature **462**: 935–939.
28. Panier S and Durocher D (2009) Regulatory ubiquitylation in response to DNA double-strand breaks. DNA repair **8**: 436–443.
29. Bekker-Jensen S, *et al* (2010) HERC2 coordinates ubiquitin-dependent assembly of DNA repair factors on damaged chromosomes. Nat Cell Biol **12**: 80–86.
30. Rossetto D, *et al* (2010) Epigenetic modifications in double-strand break DNA damage signaling and repair. Clin Cancer Res **16**: 4543–4552.
31. Morgan WF, *et al* (1996) Genomic instability induced by ionizing radiation. Radiat Res **146**: 247–258.
32. Littel JB (2003) Genomic instability and bystander effects: a historical perspective. Oncogene **22**: 6978–6987.
33. Lorimore SA, Coates PJ and Wright EG (2003) Radiation-induced genomic instability and bystander effects: inter-related nontargeted effects of exposure of exposure to ionizing radiation. Oncogene **22**: 7058–7069.
34. Suzuki K, *et al* (2003) Radiation-induced DNA damage and delayed induced genomic instability. Oncogene **22**: 6988–6993.
35. Yin B, Savic V and Bassing CH (2007) ATM prevents unattended DNA double strand breaks on site and in generations to come. Cancer Biol **6**: 1837–1839.
36. White JS, Choi S and Bakkenist CJ (2008) Irreversible chromosome damage accumulates rapidly in the absence of ATM kinase activity. Cell cycle **7**: 1277–1284.
37. Eccles LJ, Lomax ME and O'Neill P (2009) Hierarchy of lesion processing governs the repair, double-strand break formation and mutability of three-lesion clustered DNA damage. Nucleic Acids Res **38**: 1123–1134.
38. Eccles LJ, O'Neill P and Lomax ME (2011) Delayed repair of radiation induced clustered DNA damage: Friend or foe? Mutat Res 711: 134–141.
39. Sutherland BM, *et al* (2002) Clustered DNA damages induced in human hematopoietic cells by low doses of ionizing radiation. J Radiat Res **43**: S149–S152.
40. Sage E and Harrison L (2011) Clustered DNA lesion repair in eularyotes: Relevance to mutagenesis and cell survival. Mutat Res **711**: 123–133.

Received on November 11, 2010
Revision received on July 26, 2011
Accepted on July 30, 2011
J-STAGE Advance Publication Date: October 14, 2011